# Full-Spectrum Correlated-*k* Distribution for Shortwave Atmospheric Radiative Transfer

DANIEL T. PAWLAK

*Department of Meteorology, The Pennsylvania State University, University Park, Pennsylvania, and Air Force Institute of Technology, Civilian Institutions Graduate Programs Division, Wright-Patterson Air Force Base, Ohio*

EUGENE E. CLOTHIAUX

*Department of Meteorology, The Pennsylvania State University, University Park, Pennsylvania*

MICHAEL F. MODEST

*Department of Mechanical Engineering, The Pennsylvania State University, University Park, Pennsylvania*

JASON N. S. COLE

*Department of Meteorology, The Pennsylvania State University, University Park, Pennsylvania*

(Manuscript received 7 January 2004, in final form 14 May 2004)

ABSTRACT

The full-spectrum correlated *k*-distribution (FSCK) method, originally developed for applications in combustion systems, is adapted for use in shortwave atmospheric radiative transfer. By weighting *k* distributions by the solar source function, the FSCK method eliminates the requirement that the Planck function be constant over a spectral interval. As a consequence, integration may be carried out across the full spectrum as long as the assumption of correlation from one atmospheric level to the next remains valid. Problems with the lack of correlation across the full spectrum are removed by partitioning the spectrum at a wavelength of 0.68 $\mu$m into two bands. The resulting two-band approach in the FSCK formalism produces broadband rms clear-sky flux and heating rate errors less than 1% and 6%, respectively, relative to monochromatic calculations and requires only 15 quadrature points per layer, which represents a 60%–90% reduction in computation time relative to other models currently in use.

An evaluation of fluxes calculated by the FSCK method in cases with idealized clouds demonstrates that gray cloud scattering in two spectral bands is sufficient to reproduce line-by-line generated fluxes. Two different approaches for modeling absorption by cloud drops were also examined. Explicitly including nongray cloud absorption in solar source function-weighted *k* distributions results in realistic in-cloud heating rates, although in-cloud heating rates were underpredicted by approximately 8%–12% as compared to line-by-line results. A gray cloud absorption parameter chosen to fit line-by-line results optimally for one cloud or atmospheric profile but applied to different cloud combinations or profiles, also closely approximated line-by-line heating rates.

## 1. Introduction

Gases in the atmosphere of earth have absorption coefficients that vary rapidly as a function of wavelength $\lambda$ or wavenumber $\eta$, changing by several orders of magnitude across the electromagnetic spectrum. As a result, the most accurate way to perform broadband radiative transfer calculations is to divide the full spectrum into nearly monochromatic wavenumber intervals ($\delta\eta \approx 10^{-4}$–$10^{-3}$ cm$^{-1}$) and to calculate atmospheric fluxes and heating rates for each of these intervals. Integrating the results over all intervals across the spectrum leads to broadband fluxes and heating rates. This approach is called line-by-line (LBL) radiative transfer. Because of the strong variability of the gas absorption coefficients across the spectrum, the LBL approach requires millions of calculations to obtain a solution for the full shortwave, or longwave, spectrum, which makes this method impractical for use in numerical weather prediction or general circulation models.

For over 20 yr the *k*-distribution technique has been used successfully as a close approximation to integrated broadband LBL calculations (e.g., Goody and Yung 1989; Lacis and Oinas 1991; Fu and Liou 1992). In the *k*-distribution technique, gas absorption coefficients *k*

*Corresponding author address:* Eugene E. Clothiaux, Department of Meteorology, The Pennsylvania State University, 503 Walker Building, University Park, PA 16802.
E-mail: cloth@essc.psu.edu

across a portion of the spectrum are sorted in magnitude to create a *k*-distribution function. The *k* distribution is then transformed into a cumulative *k* distribution, *g*, which is a smooth monotonic function representing an equivalent nondimensional wavenumber. Both the *k* and cumulative *k* distributions contain essentially the same information for integrated radiative transfer calculations as the rapidly varying absorption coefficients versus wavenumber (e.g., Liou 2002) because the integration is independent of the ordering of the absorption coefficients. However, instead of requiring hundreds of thousands of calculations to cover the relevant portion of the spectrum in flux and heating rate calculations, the cumulative *k* distribution can be integrated with only a few quadrature points because of its smoothness.

The *k*-distribution method is exact for a homogeneous atmosphere. To account for the vertical inhomogeneity of the atmosphere, in the *correlated k*-distribution method it is assumed that absorption coefficients at different pressures and temperatures are correlated (e.g., Liou 2002). Essentially, this means that the absorption coefficient in a spectral interval, $\delta\eta$, at one atmospheric level has the same relative position in the cumulative *k* distribution as the absorption coefficients in the spectral interval at every other level, ensuring that the relative sorting of absorption coefficients from $\eta$ space to *g* space is consistent from level to level. Conditions that cause the relative sorting to change between atmospheric levels result in a breakdown of correlation and introduce error into the integration in *g* space.

A limitation of the *k*-distribution and correlated *k*-distribution methods is that the Planck function, representing either internal or external emission or both, must be nearly constant over the spectral interval of interest (e.g., Goody and Yung 1989). Although the Planck function varies smoothly, it covers a range of several orders of magnitude across the spectrum. Thus, in broadband radiative transfer calculations, cumulative *k* distributions are typically constructed for a number of spectral bands ($\Delta\eta \approx 250$–$12\,000$ cm$^{-1}$) over which the Planck function or solar source function may be assumed to be approximately constant (e.g., Fu and Liou 1992; Mlawer and Clough 1997, 1998; Kato et al. 1999). Since integration of each cumulative *k* distribution requires a few quadrature points, integration of the full spectrum requires about 40–150 quadrature points per layer depending on the particular model (e.g., Fu and Liou 1992; Mlawer and Clough 1997, 1998; Kato et al. 1999), which is still a considerable computational savings over LBL calculations. However, even considering the computational efficiency of the *k*-distribution technique, radiation calculations in numerical weather prediction models and general circulation models still require substantial computational time relative to all other physical and dynamical calculations. As a result, radiation subroutines in operational models are usually invoked far less often than the time scale on which clouds evolve in the models. If the number of calculations could be further reduced, the savings in computational time could be used to call the radiation subroutines on a time scale that would allow a more realistic interaction between radiation and clouds.

The problem of computational efficiency of radiative transfer calculations is not restricted to atmospheric applications. The full-spectrum correlated *k*-distribution (FSCK) method was developed to address the problem of radiative heat transfer in combustion systems (Modest and Zhang 2002; Modest 2003). The FSCK method eliminates the need for a constant Planck function across each spectral region to be considered in a radiative transfer calculation. In the FSCK method the cumulative *k* distribution, *g*, is no longer equivalent to a nondimensional wavenumber. Instead, by weighting the *k* distribution by the Planck function, *g* becomes equivalent to a fractional Planck function. This modification permits sorting of *k* coefficients across bands as large as the full spectrum as long as the condition of correlation between vertical atmospheric levels (discussed in sections 2 and 3) is still met. By eliminating the necessity for multiple spectral bands in broadband calculations, the total number of calculations can be reduced substantially without losing significant accuracy relative to broadband LBL calculations.

In the case of a purely external source of radiation, such as solar radiation interacting with the atmosphere of earth, the method is simplified because the only emission is at the top boundary. However, the sun does not radiate precisely as a blackbody; that is, the radiation from the sun interacting with earth's atmosphere is not precisely represented by a Planck function evaluated at the sun's effective surface temperature. Since estimates of solar irradiance are available (Kurucz 1992), the solar source function can be used as a weighting function for the *k* distribution rather than the Planck function. Because traditional *k*-distribution models assume a constant Planck function over each spectral interval to be integrated, by explicitly accounting for the spectral variability of the solar source function, the FSCK method has the potential to improve the accuracy of calculations as well.

In section 2 the FSCK method will be developed and the equations will be simplified for the solar irradiation case. A series of idealized nonhomogeneous atmospheres, which are the basis for all of our tests, will be presented in section 2. The first cases presented include only the effects of gaseous absorption with zero surface albedo. Later, cases with nonzero surface albedo, molecular (''Rayleigh'') scattering, and idealized low and high clouds in three different atmospheres are presented, including two different treatments of cloud absorption, that is, nongray and gray. In each of the cases, FSCK broadband shortwave fluxes and heating rates are compared to LBL calculations. The final section discusses our conclusions based on the results of the previous section.

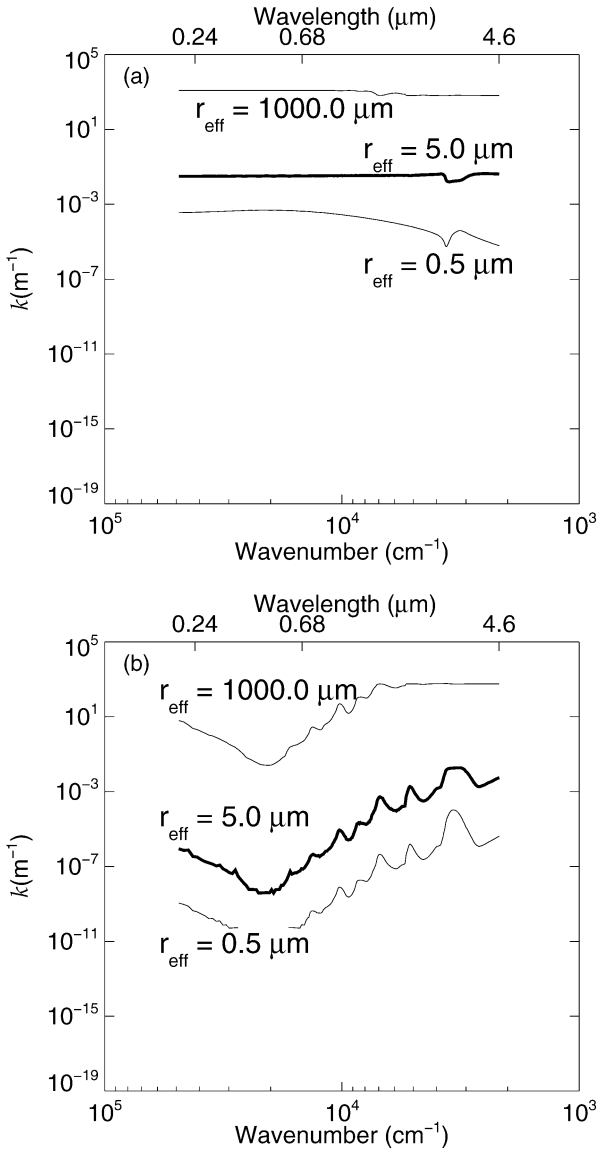


FIG. 1. Absorption and scattering coefficients for effective radii $r_{\text{eff}}$, of lognormal distribution of liquid water drops with a number concentration of 300.0 cm$^{-3}$: (a) scattering coefficient and (b) absorption coefficient.

## 2. Model background

The correlated *k*-distribution and FSCK methods are similar. In both methods the strongly variable absorption coefficients, *k*, are sorted into smooth, monotonically increasing cumulative *k* distributions, which can be integrated with a few calculations. In the correlated *k*-distribution method, however, the spectral range of the absorption coefficients to be sorted is limited by the fact that the Planck function must be constant over that range, while in the FSCK method there is no Planck function–related restriction on the spectral range to be sorted. Derivations of the two methods by Modest (2003) demonstrate the difference between the correlated *k*-distribution and FSCK methods. Because the FSCK method is further developed here for the specific case of solar radiation in the earth's atmosphere, the derivation of the FSCK method (Modest 2003) is reproduced for convenience with slight changes in the notation to make it more consistent with atmospheric radiation nomenclature.

### a. Full-spectrum correlated k-distribution method

The FSCK method extends the correlated *k*-distribution approach by relaxing the constraint that the Planck function be constant across the interval $\Delta\eta$. As a result, in the FSCK approach $\Delta\eta$ can now be arbitrarily large, even the full spectrum, as long as the scattering coefficients and phase functions are reasonably treated as constants across $\Delta\eta$. This is a significant enhancement to the correlated *k*-distribution approach, especially for spectral regions in which cloud scattering coefficients do not vary strongly with wavenumber, (e.g., Fig. 1a), while cloud absorption coefficients do (e.g., Fig. 1b).

The differential form of the radiative transfer equation for an absorbing, emitting, and scattering medium is, after Modest (2003),

$$\frac{dI(s, \mathbf{\Omega}, \eta)}{ds} = -\{k_a[\underline{\varphi}(s), \eta] + k_s[\underline{\varphi}(s), \eta]\} I(s, \mathbf{\Omega}, \eta) + k_a[\underline{\varphi}(s), \eta] B[T(s), \eta] + \frac{k_s[\underline{\varphi}(s), \eta]}{4\pi} \times \int_{\mathbf{\Omega}'} I(s, \mathbf{\Omega}', \eta) p[\underline{\varphi}(s), \mathbf{\Omega}', \mathbf{\Omega}, \eta]\, d\mathbf{\Omega}', \tag{1}$$

where $s$ is position; $I$ is monochromatic radiance; $B$ is the Planck function; $T$ is temperature; $k_a$ and $k_s$ are absorption and scattering coefficients; $p$ is the scattering phase function; $\underline{\varphi}$ is an array of state variables, including pressure, temperature, and mixing ratios; $\mathbf{\Omega}$ and $\mathbf{\Omega}'$ are solid angles; and $\eta$ is wavenumber. Assuming that the absorption coefficients are correlated across states $\underline{\varphi}$, the set of wavenumbers $\eta$ for which $k_a(\underline{\varphi}_0, \eta)$ equals some value $k$, where $\underline{\varphi}_0$ is an arbitrary reference state, must also be the set of wavenumbers $\eta$ for which $k_a(\underline{\varphi}, \eta)$ equals some value $k^*$. Since the mapping to $k^*$ depends upon both $\underline{\varphi}$ and $\eta$, or alternatively $k$, we write $k^*$ as a function $k_a^* = k_a^*(\underline{\varphi}, k)$. This mapping is represented mathematically by multiplying Eq. (1) by the Dirac delta function $\delta[k - k_a(\underline{\varphi}_0, \eta)]$. Integrating over $\Delta\eta$, which can be as large as the full spectrum as long as the condition of correlation is valid and scattering properties are approximately constant, we now have

$$\frac{dI_k(s, \mathbf{\Omega})}{ds} = -\{k_a^*[\underline{\varphi}(s), k] + k_s[\underline{\varphi}(s)]\}I_k(s, \mathbf{\Omega}) + k_a^*[\underline{\varphi}(s), k]f[T(s), \underline{\varphi_0}, k]B_{\Delta\eta}[T(s)] + \frac{k_s[\underline{\varphi}(s)]}{4\pi}\int_{\mathbf{\Omega}'} I_k(s, \mathbf{\Omega}')p[\underline{\varphi}(s), \mathbf{\Omega}', \mathbf{\Omega}]\, d\mathbf{\Omega}', \quad (2)$$

where $B_{\Delta\eta}[T(s)]$ is the Planck function integrated over the spectral interval $\Delta\eta$, and where

$$I_k(s, \mathbf{\Omega}) = \int_{\Delta\eta} I(s, \mathbf{\Omega}, \eta)\delta[k - k_a(\underline{\varphi_0}, \eta)]\, d\eta, \quad (3)$$

and

$$f[T(s), \underline{\varphi_0}, k] = \frac{1}{B_{\Delta\eta}[T(s)]}\int_{\Delta\eta} B[T(s), \eta]\delta[k - k_a(\underline{\varphi_0}, \eta)]\, d\eta. \quad (4)$$

Note that to eliminate the requirement that the Planck function must be constant over the spectral interval being sorted, the $k$ distribution is redefined using the Planck function as a weighting function; that is, the $k$ distribution has gained temperature dependence through the Planck function.

In terms of the temperature-dependent $k$ distribution the cumulative distribution function becomes

$$g[T(s), \underline{\varphi_0}, k] = \int_0^k f[T(s), \underline{\varphi_0}, k']\, dk' = \int_0^{k^*} f[T(s), \underline{\varphi}, k^{*\prime}]\, dk^{*\prime} = g[T(s), \underline{\varphi}, k^*]. \quad (5)$$

The temperature dependence of the $k$ distribution in Eq. (4) is problematic, as it introduces a dependence on location $s$ into the $k$ distribution. If we were to transform from $k$ to $g$ in Eq. (2), we would no longer be able to define $I_g = I_k/f[T(s), \underline{\varphi_0}, k]$ as the dependence of $f$ on $s$ precludes us from bringing $f$ inside the derivative on the left-hand side of the equation. To circumvent this problem Modest and Zhang (2002) use an arbitrary reference temperature, $T_{\text{ref}}$, to create a reference cumulative $k$-distribution function:

$$g_{\text{ref}}(T_{\text{ref}}, \underline{\varphi_0}, k) = \int_0^k f(T_{\text{ref}}, \underline{\varphi_0}, k')\, dk' = \int_0^{k^*} f(T_{\text{ref}}, \underline{\varphi}, k^{*\prime})\, dk^{*\prime} = g(T_{\text{ref}}, \underline{\varphi}, k^*), \quad (6)$$

where $T_{\text{ref}}$ refers to the temperature at which the Planck function is evaluated in Eq. (4). Dividing Eq. (2) by Eq. (4) with the temperature $T$ evaluated at $T_{\text{ref}}$, we obtain

$$\frac{dI_{g_{\text{ref}}}(s, \mathbf{\Omega})}{ds} = \{k_a^*[\underline{\varphi}(s), g_{\text{ref}}] + k_s[\underline{\varphi}(s)]\}I_{g_{\text{ref}}}(s, \mathbf{\Omega}) + k_a^*[\underline{\varphi}(s), g_{\text{ref}}]a[T(s), T_{\text{ref}}, g_{\text{ref}}]B_{\Delta\eta}[T(s)] + \frac{k_s[\underline{\varphi}(s)]}{4\pi}\int_{\mathbf{\Omega}'} I_{g_{\text{ref}}}(s, \mathbf{\Omega}')p[\underline{\varphi}(s), \mathbf{\Omega}', \mathbf{\Omega}]\, d\mathbf{\Omega}', \quad (7)$$

where

$$I_{g_{\text{ref}}}(s, \mathbf{\Omega}) = \frac{I_k(s, \mathbf{\Omega})}{f(T_{\text{ref}}, \underline{\varphi_0}, k)} \quad \text{and} \quad (8)$$

$$a[T(s), T_{\text{ref}}, g_{\text{ref}}] = \frac{f[T(s), \underline{\varphi_0}, k]}{f(T_{\text{ref}}, \underline{\varphi_0}, k)} = \frac{dg[T(s), \underline{\varphi_0}, k]}{dg_{\text{ref}}(T_{\text{ref}}, \underline{\varphi_0}, k)}. \quad (9)$$

In Eq. (9) $a[T(s), T_{\text{ref}}, g_{\text{ref}}]$ is a nongray stretching parameter (Modest 2003). For notational convenience we replace $g_{\text{ref}}$ with $g$ and write the absorption coefficient as $k_a^*(T_{\text{ref}}, \underline{\varphi}, g)$ to indicate explicitly that the absorption coefficients are evaluated according to the local state variables, $\underline{\varphi}$, and are subsequently weighted in the $k$ distribution by a Planck function evaluated at the reference temperature $T_{\text{ref}}$. With these changes we have

$$\frac{dI_g(s, \mathbf{\Omega})}{ds} = -\{k_a^*[T_{\text{ref}}, \underline{\varphi}(s), g] + k_s[\underline{\varphi}(s)]\}I_g(s, \mathbf{\Omega}) + k_a^*[T_{\text{ref}}, \underline{\varphi}(s), g]a[T(s), T_{\text{ref}}, g]B_{\Delta\eta}[T(s)] + \frac{k_s[\underline{\varphi}(s)]}{4\pi}\int_{\mathbf{\Omega}'} I_g(s, \mathbf{\Omega}')p[\underline{\varphi}(s), \mathbf{\Omega}', \mathbf{\Omega}]\, d\mathbf{\Omega}'. \quad (10)$$

### *b. Solar radiation*

In the special case of no internal source of emission the second term of Eq. (10) is negligible, so Eq. (10) becomes

$$\frac{dI_g(s, \mathbf{\Omega})}{ds} = -\{k_a^*[T_{\text{ref}}, \underline{\varphi}(s), g] + k_s[\underline{\varphi}(s)]\}I_g(s, \mathbf{\Omega}) + \frac{k_s[\underline{\varphi}(s)]}{4\pi}\int_{\mathbf{\Omega}'} I_g(s, \mathbf{\Omega}')p[\underline{\varphi}(s), \mathbf{\Omega}', \mathbf{\Omega}]\, d\mathbf{\Omega}'. \quad (11)$$

This formulation of the radiative transfer equation is identical to what we would obtain for the transfer of solar radiation through the atmosphere of earth with no internal source of radiation and $T_{\text{ref}}$ set to the temperature of the sun $T_{\text{sun}}$. To demonstrate this point the boundary conditions for an external solar source are

$$I^{\downarrow}(s_{\text{top}}, \mathbf{\Omega}_{\text{in}}, \eta) = I^{\downarrow}_{\text{sun}}(s_{\text{top}}, \mathbf{\Omega}', \eta)\delta(\mathbf{\Omega}' - \mathbf{\Omega}_{\text{in}}) \quad (12a)$$

for the downward radiance at the top of the atmosphere (i.e., location $s_{\text{top}}$) and

$$I^{\uparrow}(0, \mathbf{\Omega}_{\text{in}}, \eta) = \left(\frac{\alpha}{\pi}\right)\int_{2\pi} I^{\downarrow}(0, \mathbf{\Omega}', \eta)(\cos\theta)\, d\mathbf{\Omega}' \quad (12b)$$

for the upward radiance at the bottom of the atmosphere (i.e., location 0), where we have assumed a Lambertian surface with albedo $\alpha$. Multiplying these boundary conditions, as well as Eq. (1) without the source term, by $\delta[k - k_a(\underline{\varphi}_0, \eta)]$ and integrating over $\Delta\eta$, we obtain

$$I^{\downarrow}_k(s_{\text{top}}, \mathbf{\Omega}_{\text{in}}) = I^{\downarrow}_{\text{sun},\Delta\eta} f(\underline{\varphi}_{\text{sun}}, k)\delta(\mathbf{\Omega}' - \mathbf{\Omega}_{\text{in}}), \quad (13a)$$

$$I^{\uparrow}_k(0, \mathbf{\Omega}_{\text{in}}) = \left(\frac{\alpha}{\pi}\right)\int_{2\pi} I^{\downarrow}_k(0, \mathbf{\Omega}')(\cos\theta)\, d\mathbf{\Omega}', \text{ and} \quad (13b)$$

$$\frac{dI_k(s, \mathbf{\Omega})}{ds} = -\{k^*_a[\underline{\varphi}(s), k] + k_s[\underline{\varphi}(s)]\}I_k(s, \mathbf{\Omega}) + \frac{k_s[\underline{\varphi}(s)]}{4\pi} \times \int_{\mathbf{\Omega}'} I_k(s, \mathbf{\Omega}')p[\underline{\varphi}(s), \mathbf{\Omega}', \mathbf{\Omega}]\, d\mathbf{\Omega}', \quad (13c)$$

where

$$I^{\uparrow\downarrow}_k(s, \mathbf{\Omega}) = \int_{\Delta\eta} I^{\uparrow\downarrow}(s, \mathbf{\Omega}, \eta)\delta[k - k_a(\underline{\varphi}_0, \eta)]\, d\eta, \quad (14)$$

$$f(\underline{\varphi}_{\text{sun}}, k) = \frac{1}{I^{\downarrow}_{\text{sun},\Delta\eta}}\int_{\Delta\eta} I^{\downarrow}_{\text{sun}}(s_{\text{top}}, \mathbf{\Omega}', \eta) \times \delta[k - k_a(\underline{\varphi}_0, \eta)]\, d\eta, \quad (15)$$

and $I^{\downarrow}_{\text{sun},\Delta\eta}$ is the integral of the solar source function over $\Delta\eta$, the broadband spectral interval of interest.

Dividing Eqs. (13) by $f(\underline{\varphi}_{\text{sun}}, k)$, which is independent of location $s$ and can be taken inside of the derivative on the left-hand side of Eq. (13c), we obtain

$$I^{\downarrow}_g(s_{\text{top}}, \mathbf{\Omega}_{\text{in}}) = I^{\downarrow}_{\text{sun},\Delta\eta}\delta(\mathbf{\Omega}' - \mathbf{\Omega}_{\text{in}}), \quad (16a)$$

$$I^{\uparrow}_g(0, \mathbf{\Omega}_{\text{in}}) = \left(\frac{\alpha}{\pi}\right)\int_{2\pi} I^{\downarrow}_g(0, \mathbf{\Omega}')(\cos\theta)\, d\mathbf{\Omega}', \quad (16b)$$

and

$$\frac{dI_g(s, \mathbf{\Omega})}{ds} = -\{k^*_a[\underline{\varphi}(s), g] + k_s[\underline{\varphi}(s)]\}I_g(s, \mathbf{\Omega}) + \frac{k_s[\underline{\varphi}(s)]}{4\pi} \times \int_{\mathbf{\Omega}'} I_g(s, \mathbf{\Omega}')p[\underline{\varphi}(s), \mathbf{\Omega}', \mathbf{\Omega}]\, d\mathbf{\Omega}', \quad (16c)$$

where

$$I_g(s, \mathbf{\Omega}) = I_k(s, \mathbf{\Omega})/f(\underline{\varphi}_{\text{sun}}, k). \quad (17)$$

The cumulative $k$-distribution function evaluated with the solar spectral distribution of radiance is

$$g(\underline{\varphi}_{\text{sun}}, k) = \int_0^k f(\underline{\varphi}_{\text{sun}}, k')\, dk'. \quad (18)$$

For an absorbing atmosphere and a gray scattering atmosphere with or without absorption, only one spectral interval for the entire spectrum is necessary if the assumption of correlation remains valid. One source of loss of correlation in gaseous absorption between two regions of space is the presence of gradients of temperature in the medium, as in the case of a combustion system. For example, at extremely high temperatures some gas absorption lines, that is, so-called *hot lines* that originate from excited transitions, are present at spectral locations where there are no lines at room temperature. Another reason for a breakdown in correlation is vertical gradients of opposite sign for mixing ratios of different absorbing species leading to a loss of correlation in the absorption coefficients with height. Examples of this occur in the atmosphere with ozone and water vapor (Figs. 2a,b), as well as with clouds and their surrounding cloud-free layers (Figs. 2b,c). High in the atmosphere (Fig. 2a), the strongest water vapor lines are similar in magnitude to ozone continuum absorption near 46 000 $\text{cm}^{-1}$, so these lines will be sorted into nearly the same part of the cumulative $k$ distribution. Lower in the troposphere (Fig. 2b), the water vapor lines are much stronger relative to ozone continuum absorption near 46 000 $\text{cm}^{-1}$, so they will be sorted into a different part of the cumulative $k$ distribution at that level. As described in the introduction, this change of the relative sorting of absorption lines between atmospheric levels results in a breakdown of correlation and introduces error into the integration in $g$ space.

An example of the manner in which the presence of clouds can violate the assumption of correlation is shown in Figs. 2b,c. In Fig. 2b, which shows absorption for a clear-sky layer, absorption at point 1 has a similar magnitude to that at point 3, and is smaller than at point 2. However, when nongray cloud absorption coefficients (Fig. 1b) are added at the same atmospheric layer (Fig. 2c), absorption at point 1 becomes greater than both points 2 and 3. So, if clear-sky absorption in this layer had been correlated with clear-sky absorption in neighboring layers, the assumption of correlation would break down in the presence of cloud. Examples of these problems relevant to this work will be discussed in more detail in section 3, along with an adaptation of the FSCK method to circumvent them.

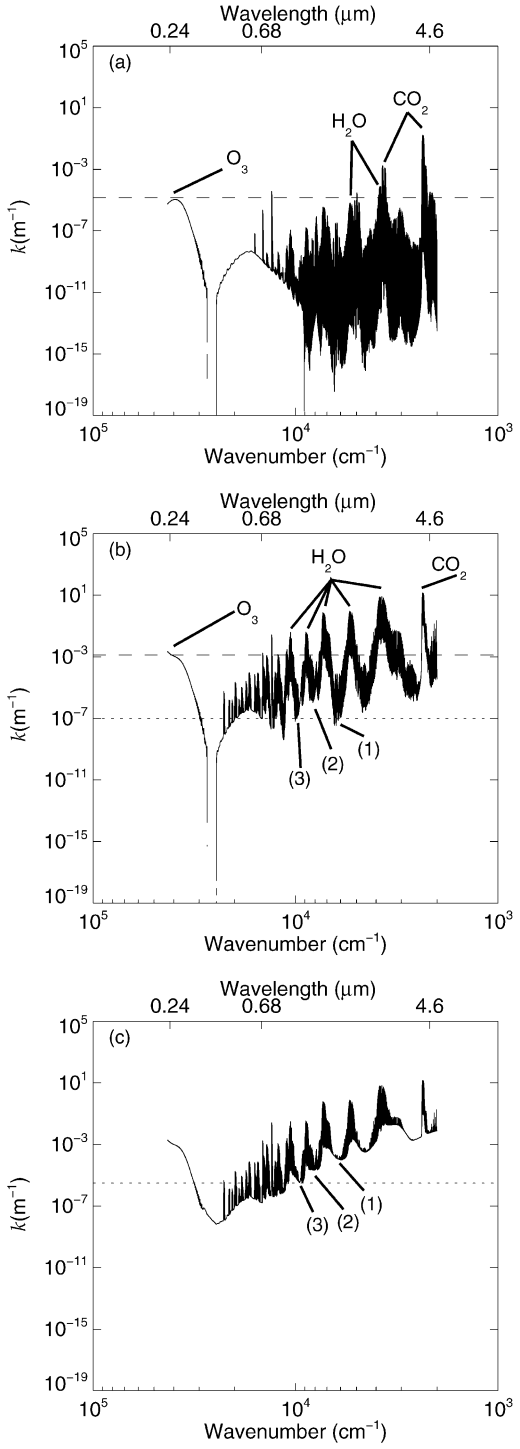


FIG. 2. Combined absorption coefficients of water vapor, carbon dioxide, ozone, nitrous oxide, carbon monoxide, methane, and oxygen at (a) 0.179 hPa and 248.2 K, (b) 841.783 hPa and 267.0 K, and (c) the same as in (b) except absorption coefficient of liquid cloud with lognormal effective radius of 5.0 $\mu$m and number concentration of 300.0 cm$^{-3}$ is added to gas absorption coefficients. The dashed line in (a) and (b) is a point of reference to compare the strengths of water vapor lines relative to ozone continuum absorption. The dotted line in (b) and (c) is a point of reference to compare the relative strengths of points 1, 2, and 3.

### c. Sorting

In practice, the method of sorting the absorption coefficients to construct the solar source function-weighted $k$ distribution and then transforming it to make the equivalent fractional solar source function–weighted cumulative $k$ distribution, $g$, is straightforward. The range of absorption coefficient values is divided into bins. To construct an ordinary $k$ distribution, we need to know the fraction, $f(k)\delta k$, of the wavenumber domain occupied by absorption coefficients in each "$k$ bin," that is, between $k$ and $k + \delta k$ (e.g., Goody and Yung 1989). When an absorption coefficient falls within a bin range, the bin count is incremented by the monochromatic wavenumber interval, $\delta\eta$, at that spectral location. If the wavenumber interval, $\delta\eta$, were constant across the spectrum, it would be sufficient to increment the bin counter by one for each occurrence within a $k$ bin. To construct a solar source function-weighted $k$ distribution (Fig. 3b), rather than incrementing the bin count by $\delta\eta$ at that spectral location, the bin count is incremented by the value of the solar source function (Fig. 3a) times $\delta\eta$ at that spectral location.

The range of values of gas absorption coefficient encountered in the McClatchey midlatitude winter atmosphere (McClatchey et al. 1972) falls between $10^{-22}$–$10^{2}$ m$^{-1}$. This range is divided into $\log_{10}(k)$ bins, with 100 bins per order of magnitude, for a total of 2401 bins. Once the solar source function-weighted $k$ distribution (Fig. 3c) is constructed, the transformation to the cumulative $k$ distribution, $g$ (Fig. 3d), is accomplished by adding up the $k$ bins, that is, $g_i = g_{i-1} + f_i \delta k_i$, where $i$ is the $k$-bin index, $f_i \delta k_i$ is the value of the $k$ distribution in the $i$th bin, and $g_{i-1}$ is the value of the cumulative $k$ distribution up to $k$-bin $i - 1$. Gaussian quadrature is typically used to integrate the cumulative $k$ distribution. The specific method of determining quadrature weights and abscissas used in this work will be discussed in section 3.

### d. Idealized atmospheres, gases, and clouds

The vertical profiles of pressure, temperature, water vapor, and ozone used for the calculations in this article are taken from the McClatchey et al. (1972) subarctic winter, midlatitude winter, and tropical atmospheres and are interpolated to 29 layers with a total of 30 layer boundaries, where the lowest 21 layers are 1 km thick, the next two layers are 2 km thick, the next five layers are 5 km thick, and the top layer is 20 km thick. The profiles of oxygen, carbon dioxide, carbon monoxide, methane, and nitrous oxide are adapted from a METEO 597A class project at The Pennsylvania State University, with volume mixing ratios and temperatures shown in Fig. 4. The gas absorption coefficients are extracted from the HITRAN-96-JPL database (Rothman et al. 1998) using the line-by-line radiative transfer model (LBLRTM) version 5.21 (Clough et al. 1992; Clough

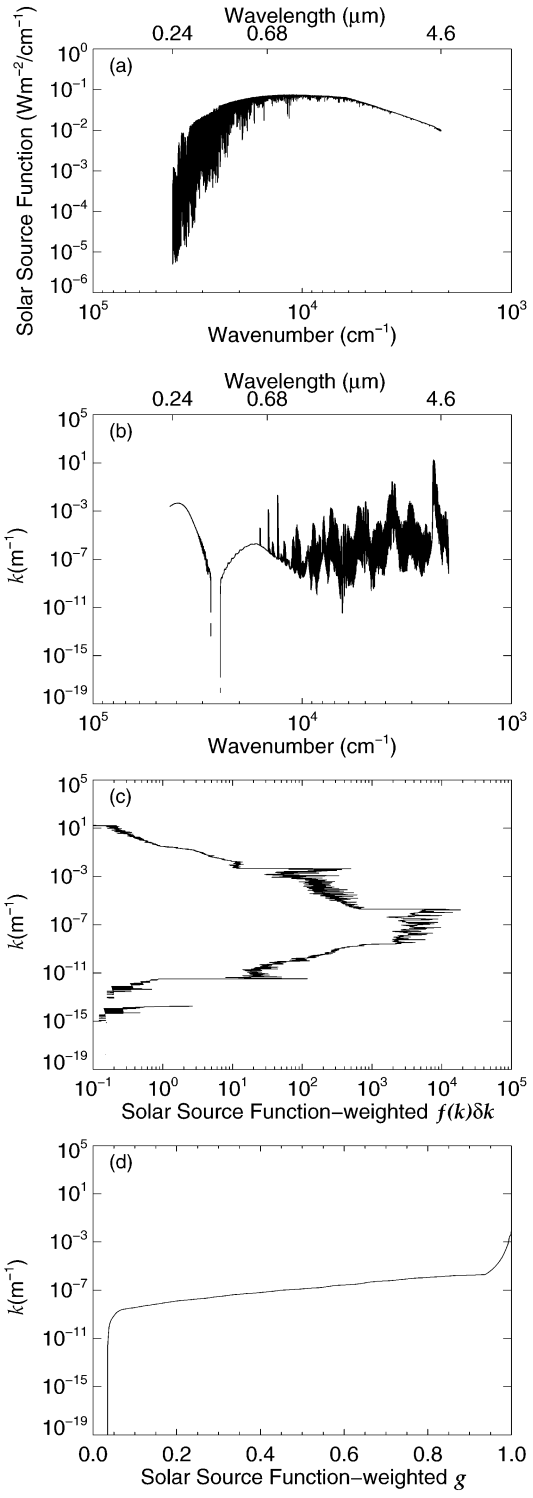


FIG. 3. (a) Solar source function; (b) combined absorption coefficients of water vapor, carbon dioxide, ozone, nitrous oxide, carbon monoxide, methane, and oxygen at 148.949 hPa and 217.9 K; (c) solar source function–weighted $k$ distribution, and (d) solar source function–weighted cumulative $k$ distribution.

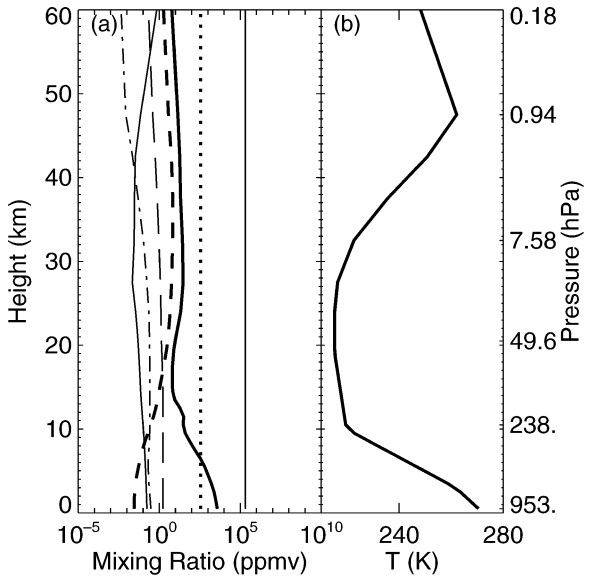


FIG. 4. (a) Gas mixing ratio (ppmv). From right to left at 30 km, oxygen (thin solid line), carbon dioxide (dotted line), water vapor (thick solid line), ozone (thick dashed line), methane (thin dashed line), nitrous oxide (dash–dot line), and carbon monoxide (dash–three dots line). (b) Temperature (K).

and Iacono 1995). Absorption coefficients for the individual gas constituents are combined by LBLRTM, so line overlap and continuum absorption are explicitly calculated prior to sorting the combined absorption coefficients.

In the cases where idealized clouds are included the optical properties of clouds are calculated using Mie theory according to Toon and Ackerman (1981) for log-normal distributions of liquid- or ice-water spheres with a logarithmic distribution width of 0.38. In our calculations, liquid-water clouds have a visible optical depths of approximately 30, while ice clouds are optically thin, with a visible optical depth of approximately 0.25. Liquid cloud-drop distributions used here have an effective radius of 5 $\mu$m. The liquid cloud in these cases, which we also call the low cloud, is homogeneously distributed between 1000–2000 m of altitude. Our ice, or high, cloud-drop distributions have an effective radius of 75 $\mu$m, and are homogeneously distributed in the layer between 7000–8000 m. The cloud optical properties used for the monochromatic line-by-line calculations were produced at a spectral resolution of 0.01 $\mu$m and then interpolated to the wavenumber resolution of the gas absorption coefficients.

In the results that follow, the two-stream solver of Zdunkowski et al. (1982) is used for the LBL flux and heating rate calculations. These LBL fluxes and heating rates represent the ''truth.'' For consistency, we also used the same solver in the FSCK calculations. Therefore, in the comparisons between the FSCK calculations and the LBL standard, differences due to model solvers are not a consideration.

## 3. Results

### *a. Clear-sky calculations*

The first idealized case is a basic test of the FSCK method versus LBL calculations. In this case there are no clouds, no molecular scattering, the surface albedo is zero, and the midlatitude winter atmospheric profile is used. The full shortwave spectrum (i.e., 0.24–4.60 $\mu$m, or 2174–41 667 cm$^{-1}$) is treated as a single spectral band, and the gas absorption coefficients are sorted into a single cumulative $k$ distribution per layer. For this initial test of the FSCK method, 8192 quadrature points are used for the integration of the cumulative $k$ distributions in order to ensure that differences between the FSCK results and the LBL calculations are not due to poor quadrature. This number was selected by doubling the number of quadrature points, starting with one, until the calculated heating rate profile ceased to change with a subsequent doubling of points.

Comparing the vertical profiles of downward fluxes and heating rates for the LBL calculations and the FSCK results (Figs. 5a–c), we find less molecular absorption in the FSCK results with the most significant differences in the lowest 15 km of the atmosphere. As shown in Figs. 2a,b, these differences result from a loss of correlation between the $k$ distributions for different vertical levels as a result of different vertical gradients in the water vapor and ozone mixing ratios (Fig. 4a). This condition is always present in the atmosphere of earth.

Since absorption by ozone is dominant in the upper atmosphere, less absorbing in the lower atmosphere relative to the other gases, and nearly the only mechanism for absorption in the spectral range from 0.24–0.68 $\mu$m (14 706–41 667 cm$^{-1}$), we separate the shortwave spectrum into two bands, with band 1 from 0.24–0.68 $\mu$m and band 2 from 0.68–4.60 $\mu$m (2174–14 706 cm$^{-1}$), and test the assumption of vertical correlation within each of these two spectral bands. The resulting fluxes and heating rates are much more accurate (Figs. 5d–l). For band 1 the maximum errors in the flux in the lowest layers of the atmosphere are less than 1% and heating rate errors are also small, being less than approximately 0.005 K day$^{-1}$ (Figs. 5d–f). We were able to find a five-point quadrature of the FSCK cumulative distribution functions for band 1 that led to nearly identical results with the 8192-point quadrature. That is, the FSCK treatment of gaseous absorption in band 1 is accurate to within approximately 3% of LBL heating rates and a five-point quadrature for this band is possible without a significant loss of accuracy.

The band-2 comparisons (Figs. 5g–i) demonstrate that the assumption of vertical correlation is also valid for the spectral interval from 0.68–4.60 $\mu$m, as the FSCK 8192-point quadrature flux and heating rate rms differences from the LBL results are less than 1% and 6%, respectively. However, for band 2, the quality of the FSCK results are highly dependent on the number of quadrature points. Using a 10-point quadrature, which represents a compromise between accuracy and computational efficiency, we found the heating rate errors in the troposphere to be less than 13%, while the errors in the stratosphere reached 66%. But, the consequence of the large percentage error in the stratosphere amounts to only a heating rate error of $\sim$1.1 K day$^{-1}$, which is small, that is, less than 6%, when the total, full spectrum heating rate is considered (Figs. 5j–l). Overall, the FSCK method produced heating rates accurate to approximately 4% in the troposphere and 3% in the stratosphere. Limiting the band-2 quadrature scheme to 10 points led to larger full-spectrum heating rate errors of 5% and 7% in the troposphere and stratosphere, respectively.

Shifted Gauss–Chebyschev II quadrature (Wang and Modest 2004) is used to calculate the weights and abscissas for band 2 (Table 1). However, there is a sharp kink present in many of the cumulative $k$ distributions of band 1 near $g = 0.95$ (not shown) that reduces the accuracy of Gaussian quadrature methods. As a result, we use trapezoidal quadrature for band 1 with weights and abscissas optimally selected to fit the LBL solution.

The next test case also consisted of the same clear-sky midlatitude winter profile, but with molecular (i.e., Rayleigh) scattering and a gray surface albedo of 0.15 included in both the FSCK and LBL calculations. For the LBL calculations we used the spectrally dependent Rayleigh scattering optical depths calculated according to Teillet (1990), while for the two-band FSCK calculations the Rayleigh scattering optical depths were calculated using the same technique but at fixed wavelengths of 0.47 $\mu$m (21 182 cm$^{-1}$) for band 1 and 0.90 $\mu$m (11 111 cm$^{-1}$) for band 2. In the FSCK calculations we also used the same 5- and 10-point quadrature values for bands 1 and 2 that we derived in the gas-absorption-only case. Not surprisingly, the flux and heating rate errors that we obtained for this case (Figs. 6a–c) do not differ in any significant way from those that we obtained for the gas-absorption-only case. Moreover, results for clear-sky calculations in subarctic winter and tropical atmospheres are similar (not shown).

### *b. Cloudy sky calculations*

The next two sets of test cases examine the accuracy of FSCK calculations in cloudy conditions. In the first case, an FSCK treatment of nongray cloud absorption with parameterized gray cloud scattering is evaluated, and in the second case, both gray cloud absorption and gray cloud scattering are parameterized. In both sets of calculations we consider the effects of low cloud, high cloud, and both low and high clouds combined. The two sets of calculations differ in the method by which we account for cloud absorption in the FSCK calculations.

In the first set of calculations, where cloud absorption is nongray and cloud scattering is gray, we interpolated the 0.01-$\mu$m-resolution cloud absorption coefficients (Fig. 1b) to the spectral resolution of the gas coefficients

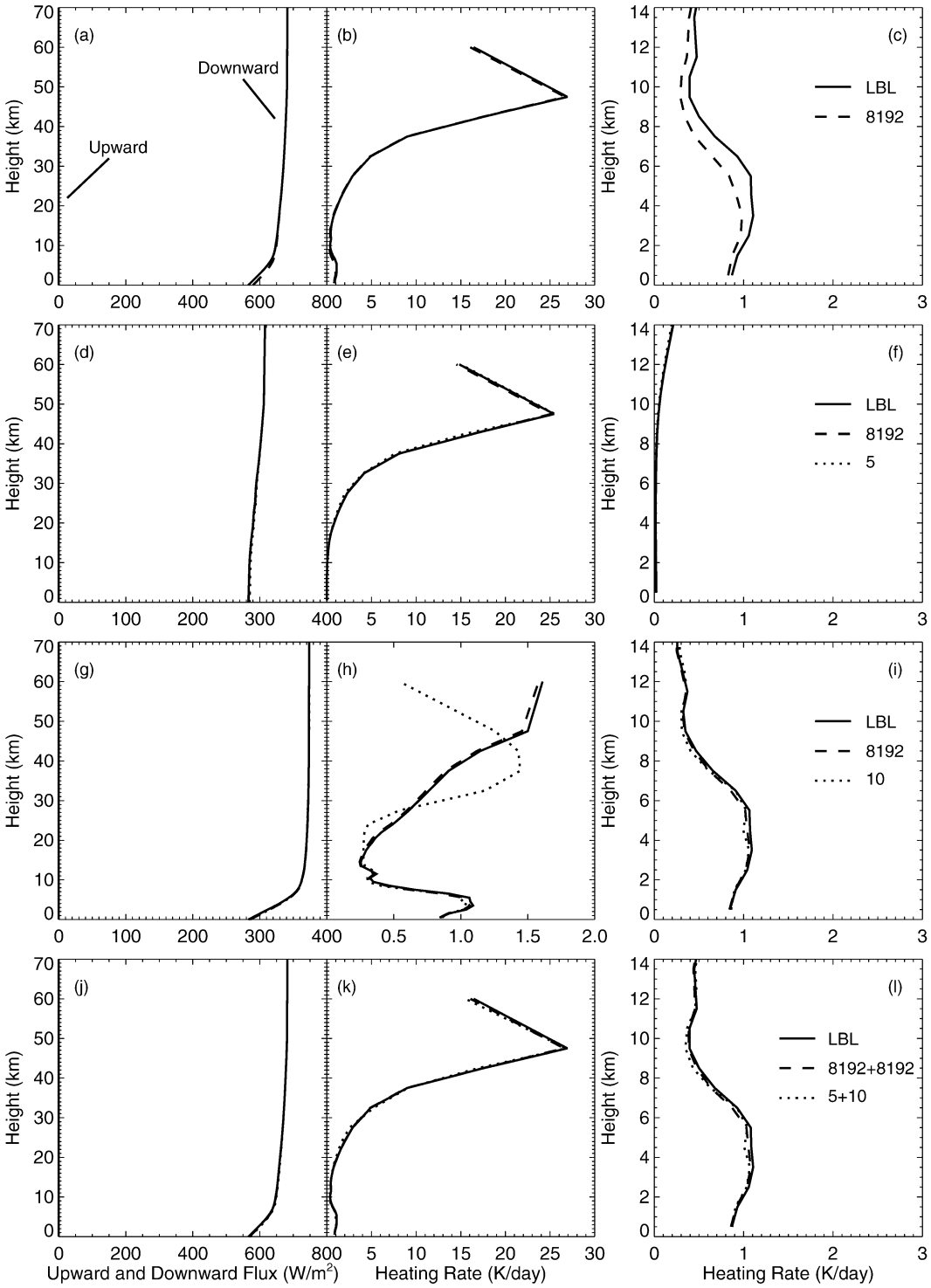


FIG. 5. (a), (d), (g), and (j) Upward and downward fluxes; (b), (e), (h), and (k) heating rates for all 29 layers; and (c), (f), (i), and (l) heating rates for the lowest 14 layers (a)–(c) for the full shortwave spectrum (0.24–4.6 $\mu$m) treated as a single band (d)–(f) band 1 (0.24–0.68 $\mu$m), (g)–(i) band 2 (0.68–4.6 $\mu$m), and (j)–(l) the full shortwave spectrum treated by adding bands 1 and 2 comparing results of the LBL solution (solid line), the 8192 quadrature point solution (dashed line), and the 15 quadrature point solution (dotted line).

TABLE 1. Trapezoidal quadrature abscissas and weights for band 1 and shifted Gauss–Chebyschev II quadrature abscissas and weights for band 2 before and after transformation.

| Band 1 | | Band 2 before transformation | | Band 2 after transformation | |
|---|---|---|---|---|---|
| Abscissa | Weight | Abscissa | Weight | Abscissa | Weight |
| 0.453 830 | 0.907 660 | 0.000 000 | 0.076 046 | 0.000 000 | 0.113 893 |
| 0.929 175 | 0.043 030 | 0.156 434 | 0.160 133 | 0.225 220 | 0.220 272 |
| 0.962 060 | 0.022 740 | 0.309 017 | 0.144 407 | 0.425 618 | 0.179 779 |
| 0.981 040 | 0.015 220 | 0.453 990 | 0.144 940 | 0.596 540 | 0.160 402 |
| 0.994 325 | 0.011 350 | 0.587 785 | 0.122 105 | 0.735 342 | 0.117 413 |
| | | 0.707 107 | 0.116 036 | 0.841 487 | 0.094 052 |
| | | 0.809 017 | 0.087 385 | 0.916 537 | 0.057 194 |
| | | 0.891 007 | 0.076 215 | 0.964 017 | 0.037 684 |
| | | 0.951 057 | 0.043 742 | 0.989 172 | 0.014 493 |
| | | 0.987 688 | 0.028 991 | 0.998 634 | 0.004 818 |

in the cloudy layers and then added the interpolated cloud absorption coefficients to the gas absorption coefficients. The combined cloud and gas absorption coefficients were then sorted to form the cumulative *k*-distribution functions from which the final 5- and 10-point quadrature *k* values for the radiative transfer were selected. The advantage of this approach is that spectral variations in the cloud absorption coefficients are explicitly taken into account. The disadvantage to this approach is that adding the cloud absorption coefficients to the gas absorption coefficients leads to a partial loss of correlation in the *k* distributions between the cloudy layers and their neighboring clear-sky layers, as we illustrated in Figs. 2b,c. The parameterized gray liquid- and ice-cloud asymmetry parameters, single scatter albedos, and scattering cross sections used for this first set of nongray cloud absorption and gray cloud scattering calculations are shown in Table 2. We obtained these values by taking a band average of the fine-spectral-resolution Mie calculations weighted by spectrally varying direct downwelling transmission at 500 hPa. The resulting parameters were fine-tuned by minimizing the flux errors between the 8192-point solution and the LBL calculations. Note that in this case nongray absorption by cloud drops is explicitly accounted for in the *k* distributions, so the gray tuning parameters are adjusted so that they do not account for cloud absorption a second time; that is, the gray cloud extinction cross section is set equal to the scattering cross section, and the single scatter albedo is set to 1.0.

As shown in Figs. 6d–f (Figs. 6g–i) for a low (high) cloud, maximum upward and downward flux errors were always less than 6% with typical errors near 1%, while the heating rate errors were generally less than 4% in the clear-sky regions above the highest cloud layer and no greater than approximately 10% in and below the cloud layer. In both the low- and high-cloud cases the FSCK simulations with nongray cloud absorption and gray cloud scattering produced slightly less heating than the LBL calculations. The cloud parameters that we obtained for the single cloud-layer cases were used for the combined low- and high-cloud case, and results of that case were consistent with the single cloud-layer cases (Figs. 6j–l). The likely source of error in this case of nongray cloud absorption is a breakdown in correlation, as described in section 2, and correlation could be partially restored by subdividing band 2 into more bands. However, we are attempting to balance accuracy with efficiency. Each additional band would require 5–10 additional quadrature points, and since the magnitude of the maximum in-cloud heating rate errors in this nongray cloud absorption case is similar in magnitude to heating rate errors of other state-of-the-art one-dimensional radiative transfer models relative to line-by-line calculations (Barker et al. 2003), we do not attempt to reduce further the two-band FSCK errors.

In the second set of calculations we treated the cloud absorption coefficient as gray within each band, in addition to gray scattering coefficients and asymmetry parameters. The values of the three parameterized gray cloud properties, that is, asymmetry parameter, single-scattering albedo, and extinction cross section, were determined as described above for the gray cloud scattering properties in the first set of calculations, except that the gray cloud extinction cross sections and single scatter albedos now account for cloud absorption. The tuning parameters for gray cloud absorption and gray cloud scattering are shown in Table 2. As the results in Figs. 7a–c and 7d–f illustrate, values for the three coefficients exist that provide accurate fluxes, to better than 3%, and heating rates, to better than 6%, for each cloudy atmosphere. These results demonstrate that relatively accurate parameterization of single cloud-layer optical properties with gray values for the two bands is possible. Note that with three tuning parameters, that is, asymmetry parameter, single scatter albedo, and extinction coefficient, flux errors might be reduced more with a different combination of these parameters. If this gray cloud absorption and gray cloud scattering approach is further developed, sets of parameters must be determined for the range of cloud particle size distributions encountered in the numerical models in which it is implemented.

Incorporating the coefficients computed separately

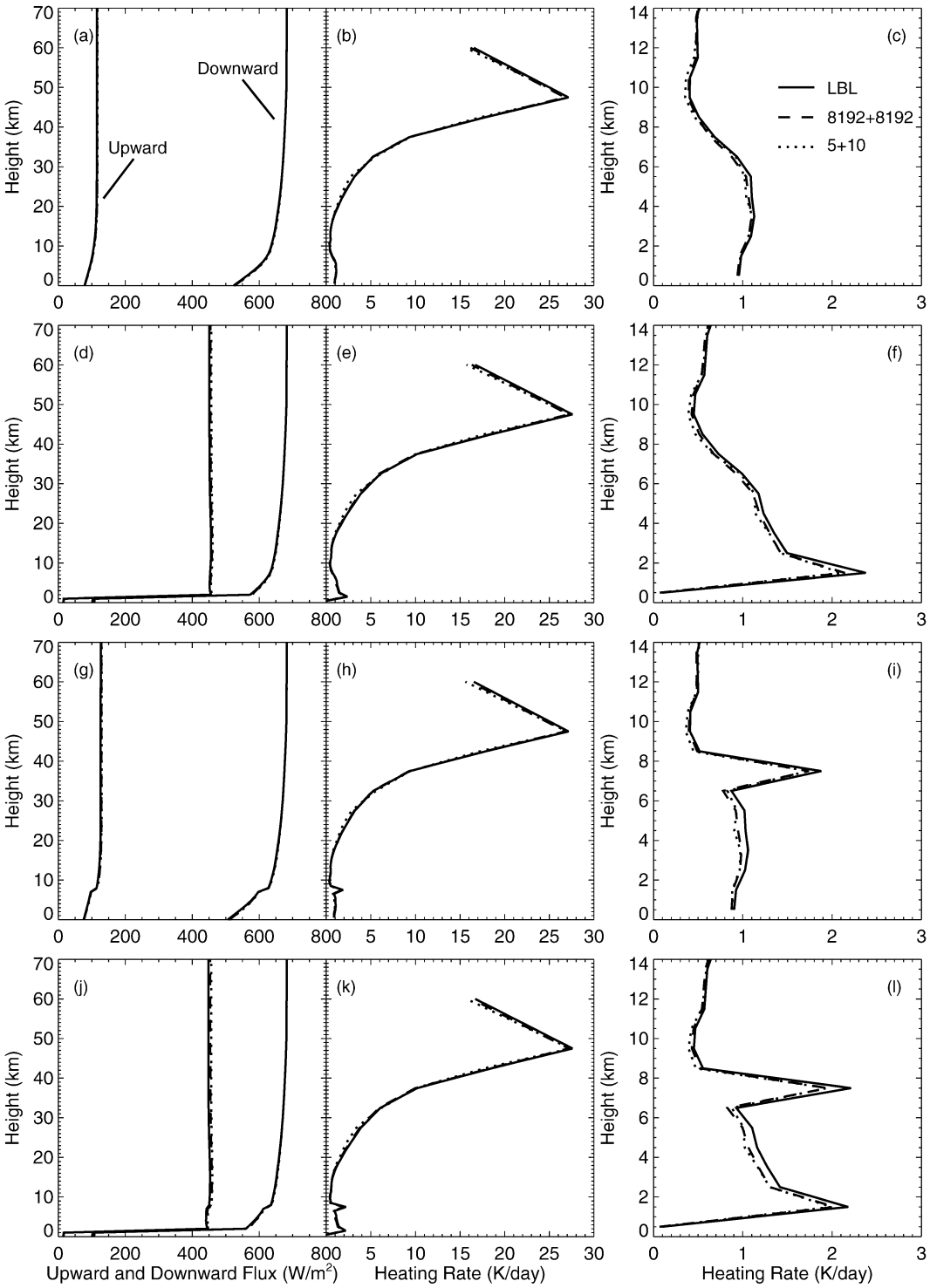


FIG. 6. (a), (d), (g), and (j) Upward and downward fluxes; (b), (e), (h), and (k) heating rates for all 29 layers; and (c), (f), (i), and (l) heating rates for the lowest 14 layers for (a)–(c) clear sky, (d)–(f) a liquid cloud with nongray absorption and gray scattering, (g)–(i) an ice cloud with nongray absorption and gray scattering, and (j)–(l) both clouds with nongray absorption and gray scattering comparing results of the LBL solution (solid line), the 8192 quadrature point solution (dashed line), and the 15 quadrature point solution (dotted line).

TABLE 2. Asymmetry parameter $g$, single scatter albedo $\omega_0$, and extinction cross section $\sigma_{ext}$ for a lognormal distribution of liquid water spheres of radius 5 $\mu$m and ice spheres of radius 75 $\mu$m for band 1 (0.24–0.68 $\mu$m) and band 2 (0.68–4.6 $\mu$m), for nongray absorption and gray scattering, and for gray absorption and gray scattering.

| | Band 1 | | | Band 2 | | |
|---|---|---|---|---|---|---|
| | $g$ | $\omega_0$ | $\sigma_{ext}$ | $g$ | $\omega_0$ | $\sigma_{ext}$ |
| Nongray absorption and gray scattering | | | | | | |
| Liquid | 0.849 | 1.000 | $1.10 \times 10^2$ | 0.825 | 1.000 | $9.40 \times 10$ |
| Ice | 0.888 | 1.000 | $2.33 \times 10^4$ | 0.898 | 1.000 | $2.35 \times 10^4$ |
| Gray absorption and gray scattering | | | | | | |
| Liquid | 0.856 | 0.999 | $1.10 \times 10^2$ | 0.800 | 0.998 | $9.30 \times 10$ |
| Ice | 0.867 | 0.999 | $2.32 \times 10^4$ | 0.898 | 0.955 | $2.34 \times 10^4$ |

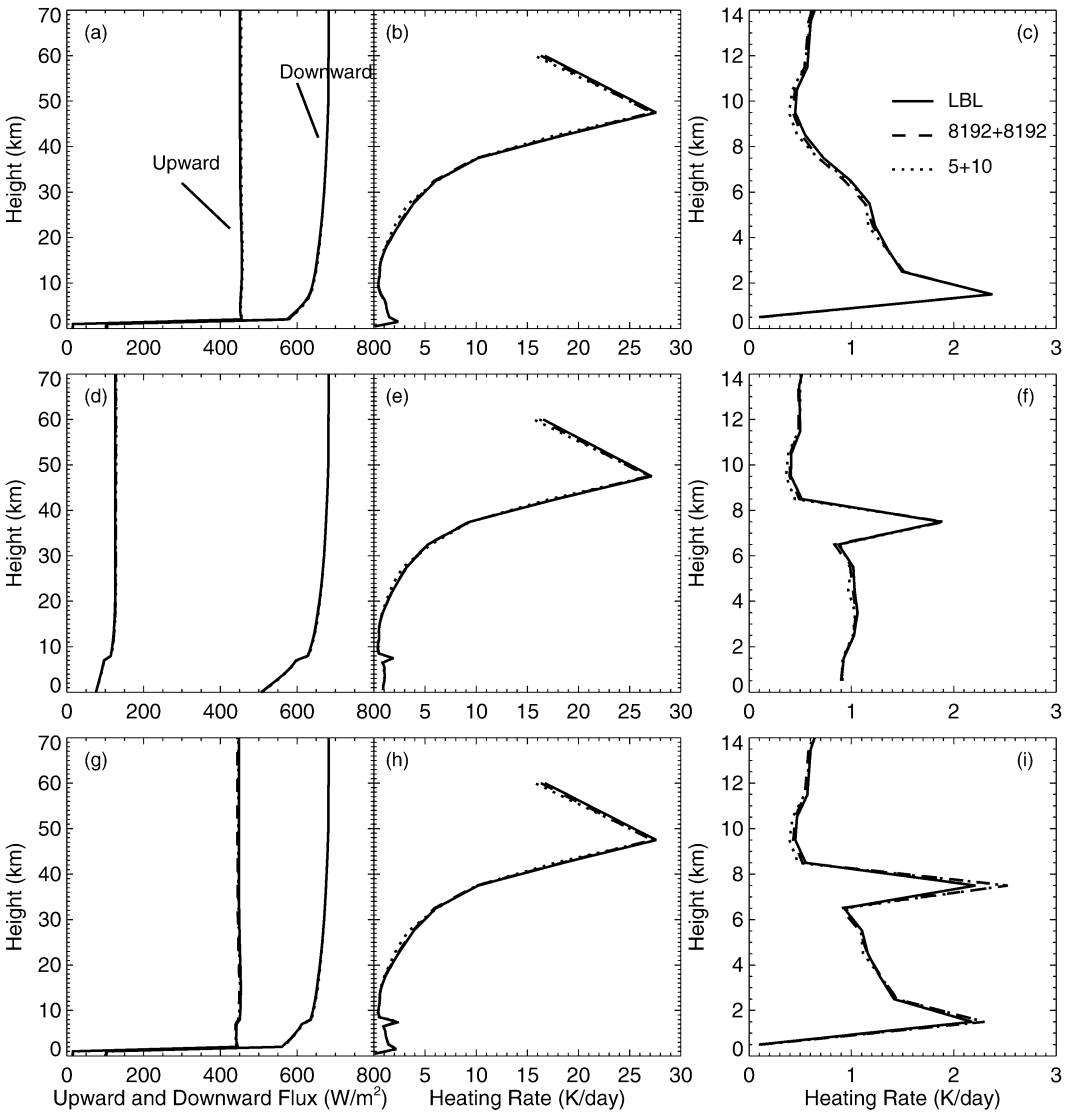


FIG. 7. (a), (d), and (g) Upward and downward fluxes; (b), (e), and (h) heating rates for all 29 layers; and (c), (f), and (i) heating rates for the lowest 14 layers for (a)–(c) a liquid cloud with gray absorption and gray scattering, (d)–(f) an ice cloud with gray absorption and gray scattering, and (g)–(i) both clouds with gray absorption and gray scattering comparing results of the LBL solution (solid line), the 8192 quadrature point solution (dashed line), and the 15 quadrature point solution (dotted line).

for the low and high clouds into a combined low- and high-cloud FSCK calculation produced flux and in-cloud heating rate errors of 1% and 10%, respectively, relative to the LBL results (Figs. 7g–i). The magnitudes of the in-cloud heating rate errors using this second approach are similar to those resulting from explicitly incorporating the nongray cloud absorption coefficients into the solar source function-weighted cumulative $k$ distributions, although the magnitudes and signs of the errors are less consistent from the single-layer to two-layer cloud cases than for the nongray cloud absorption calculations.

As we just demonstrated, the two sets of FSCK calculations for the midlatitude winter atmosphere produced comparable results, with errors both in the fluxes and in the heating rates of similar magnitudes. Performing identical sets of calculations for both the subarctic winter and tropical atmospheres, with the same quadrature points and cloud parameters derived for the midlatitude winter atmosphere, we obtained results consistent with those from the midlatitude winter atmosphere calculations.

## 4. Discussion and conclusions

The flux and heating rate results obtained in this study demonstrate that the full-spectrum correlated $k$-distribution (FSCK) method is an accurate and efficient alternative to line-by-line (LBL) calculations for shortwave atmospheric radiative transfer. By weighting $k$ distributions by the Planck function, or by the solar source function in the case of solar radiation, the FSCK method eliminates the requirement that the Planck function, or solar source function, be constant over the spectral intervals to be integrated. Consequently, a spectral band may be arbitrarily large in the FSCK approach, even encompassing the full spectrum, as long as the assumption of correlation in the gas absorption coefficients between regions of the atmosphere remains valid. As a result of the vertical distribution of absorbing gases in the atmosphere, primarily ozone and water vapor, the correlation assumption breaks down when the full shortwave spectrum is treated as a single band. However, the breakdown of correlation may be circumvented by separating the spectrum into two bands at a wavelength of 0.68 $\mu$m (14 706 cm$^{-1}$), separating the spectrum into two regions, that is, one in which ozone continuum absorption is more important, and the other where it is less important relative to absorption by other gases.

Comparisons of two-band FSCK and LBL results indicate that the broadband FSCK clear-sky fluxes and heating rates are accurate to better than 1% and 3%, respectively, when 8192 quadrature points are used within each band. Limiting the first band from 0.24–0.68 $\mu$m to 5 quadrature points and the second band from 0.68–4.60 $\mu$m to 10 quadrature points, the accuracies of the FSCK fluxes and heating rates become approximately 1% and 7%, respectively. For idealized low- and high-cloud test cases we found that gray cloud scattering for the two spectral bands with 5- and 10-point quadratures is sufficient to reproduce the LBL-generated fluxes and heating rates, which used spectrally varying cloud absorption and scattering properties, to approximately 1% and 8%, respectively. Two different approaches to modeling absorption by cloud drops were examined. Explicitly including spectrally varying cloud absorption into the solar source function-weighted $k$ distributions resulted in realistic in-cloud heating rates, although the heating rates were consistently less than LBL-calculated rates. Gray cloud absorption parameters that were chosen to optimally fit LBL results for one atmosphere, but applied to different atmospheres or cloud combinations, also closely approximated LBL in-cloud heating rates, although the heating rate errors were less consistent in magnitude and sign than in the first approach as cloud layers were combined.

The FSCK solution requires only 15 quadrature points per layer, a 60%–90% reduction in computational overhead from other models currently in use (e.g., Fu and Liou 1992; Mlawer and Clough 1998; Kato et al. 1999). Hence, the FSCK method is potentially important to numerical modeling of radiative transfer, because the computational burden of the radiative transfer calculations is strongly linked to the number of spectral bands required. The next step in the application of the FSCK method to shortwave atmospheric radiative transfer is to develop a robust radiative transfer module that may be used in operational numerical weather prediction or global climate models. This will require additional testing on nonidealized cloud fields to assess FSCK heating rate errors under a variety of atmospheric conditions. Furthermore, direct comparisons between the FSCK method and current models will be required to determine the relative accuracy of the models, but by explicitly accounting for spectral variability of the solar source function, the FSCK method has the potential for improving accuracy relative to traditional correlated $k$-distribution models that assume constant solar emission over each band. An extension of the FSCK method to longwave atmospheric radiative transfer is also being developed.

*Acknowledgments.* This work was supported by the Department of Energy Atmospheric Radiation Measurement program (under Grant DE-FG02-90ER61071) and the Air Force Institute of Technology Civilian Institutions program. The views expressed in this article are those of the authors and do not reflect the official policy or position of the United States Air Force, Department of Defense, or the U.S. Government. The authors would like to thank Anthony Clough, Eli Mlawer, and Jennifer Delamere for their support and comments as we used their monochromatic radiative transfer code LBLRTM, and Seiji Kato and Howard Barker for many discussions on correlated $k$-distribution issues in atmospheric science research. The authors would also like

to thank the following class participants in The Pennsylvania State University seminar METEO 597A for compiling the profiles of atmospheric gases used in Fig. 4a: Matt Boehm, Brian Etherton, Laura Hinkleman, Urszula Jambor, Mike Jenson, Ricardo Muñoz, Chuck Pavloski, and Manajit Sengupta. Two anonymous reviewers caught inconsistencies in our original manuscript, and we are grateful for their having done so.

## REFERENCES

Barker, H. W., and Coauthors, 2003: Assesing 1D atmospheric solar radiative transfer models: Interpretation and handling of unresolved clouds. *J. Climate,* **16,** 2676–2699.

Clough, S. A., and M. J. Iacono, 1995: Line-by-line calculation of atmospheric fluxes and cooling rates, 2, Application to carbon dioxide, ozone, methane, nitrous oxide, and the halocarbons. *J. Geophys. Res.,* **100,** 16 519–16 535.

——, ——, and J.-L. Moncet, 1992: Line-by-line calculation of atmospheric fluxes and cooling rates: Application to water vapor. *J. Geophys. Res.,* **97,** 15 761–15 785.

Fu, Q., and K. N. Liou, 1992: On the correlated *k*-distribution method for radiative transfer in non-homogeneous atmospheres. *J. Atmos. Sci.,* **49,** 2139–2156.

Goody, R. M., and Y. L. Yung, 1989: *Atmospheric Radiation—Theoretical Basis.* 2d ed. Oxford University Press, 519 pp.

Kato, S., T. P. Ackerman, J. H. Mather, and E. E. Clothiaux, 1999: The *k*-distribution method and correlated-*k* approximation for a shortwave radiative transfer model. *J. Quant. Spectrosc. Radiat. Transfer,* **62,** 109–121.

Kurucz, R. L., 1992: Synthetic infrared spectra. *Infrared Solar Physics: Proceedings of the 154th IAU Symposium,* D. M. Rabin and J. T. Jeffries, Eds., Kluwer Academic, 523–531.

Lacis, A. A., and V. Oinas, 1991: A description of the correlated *k* distribution method for modeling nongray gaseous absorption, thermal emission, and multiple scattering in vertically inhomogeneous atmospheres. *J. Geophys. Res.,* **96** (D5), 9027–9063.

Liou, K. N., 2002: An *Introduction to Atmospheric Radiation.* 2d ed. Academic Press, 583 pp.

McClatchey, R. A., R. W. Fenn, J. E. A. Selby, F. E. Volz, and J. S. Garing, 1972: Optical properties of the atmosphere. 3d ed. AFCRL-72-0497, Air Force Cambridge Research Laboratories, Bedford, MA, 108 pp.

Mlawer, E. J., and S. A. Clough, 1997: On the extension of rapid radiative transfer model to the shortwave region. *Proc. Sixth Amospheric Radiation Measurement (ARM) Science Team Meeting,* San Antonio, TX, U.S. Department of Energy, CONF-9603149, 223–226.

——, and ——, 1998: Shortwave and longwave enhancements in the rapid radiative transfer model. *Proc. Seventh Amospheric Radiation Measurement (ARM) Science Team Meeting,* San Antonio, TX, U.S. Department of Energy, CONF-970365, 409–413.

Modest, M. F., 2003: Narrow-band and full-spectrum *k*-distributions for radiative heat transfer-correlated-*k* vs. scaling approximation. *J. Quant. Spectrosc. Radiat. Transfer,* **76,** 69–83.

——, and H. Zhang, 2002: The full-spectrum correlated *k*-distribution for thermal radiation from molecular gas-particulate mixtures. *ASME J. Heat Transfer,* **124,** 30–38.

Rothman, L. S., and Coauthors, 1998: The HITRAN molecular spectroscopic database and HAWKS (HITRAN Atmospheric Workstation): 1996 edition. *J. Quant. Spectrosc. Radiat. Transfer,* **60,** 665–710.

Teillet, P. M., 1990: Rayleigh optical depth comparisons from various sources. *Appl. Opt.,* **29,** 1897–1900.

Toon, O. B., and T. Ackerman, 1981: Algorithms for the calculation of scattering by stratified spheres. *Appl. Opt.,* **20,** 3657–3660.

Wang, A., and M. F. Modest, 2004: High-accuracy, compact database of narrow-bank *k*-distributions for water vapor and carbon dioxide. *Proc. ICHMT Fourth Int. Symp. on Radiative Transfer,* Istanbul, Turkey, ICHMT.

Zdunkowski, W. G., W.-G. Panhans, R. M. Welch, and G. J. Korb, 1982: A radiation scheme for circulation and climate models. *Contrib. Atmos. Phys.,* **55,** 215–238.